Proceedings of the 12th International Conference on
Aluminium Alloys, September 5-9, 2010, Yokohama, Japan

pp. 2432-2437

Improving the Mechanical Performance of a Secondary Cast Aluminium Piston Alloy through Addition of Minor Elements

T. O. Mbuya[1], B. R. Mose[2], S.P. Ng'ang'a[2] and S. M. Maranga[2]
[1]Department of Mechanical and Manufacturing Engineering, University of Nairobi, Kenya
[2]Department of Mechanical Engineering, Jomo Kenyatta University of Agriculture and Technology, Kenya

Abstract: The effect of minor element additions (Sr, Sb, Mn, Cr and Al-5Ti-1B grain refiner) on the mechanical performance of a secondary cast aluminium piston alloy, with 1 wt.% Fe was investigated. It was observed that addition of even high levels of Cr of up to 1% was better than a 0.53%Mn addition in improving the tensile strength, impact energy and % elongation of the alloy. The high mechanical performance recorded in the 1%Cr alloy was attributed to its low porosity compared to all other alloys and the fine compact intermetallics observed in the alloy. Other additions also resulted in improved mechanical properties with 0.53%Mn performing better than 0.3%Mn+0.2%Cr while 0.02%Sr, 0.05%Sr, 0.02%Sr+0.53%Mn, 0.05%Sr+0.53%Mn, 0.2Sb and 0.2Sb+0.53%Mn recording marginal improvements.

Keywords: *Al-Si Alloy, Mechanical Properties, Aluminium Recycling, Si Modification, Fe-rich Intermetallics.*

1. Introduction

Cast Al-Si alloys have found widespread use in aerospace and ground transportation vehicles. They are, for example, the preferred choice for light vehicle engine pistons that work in a highly demanding service environment of fluctuating temperature and pressure. Al-Si Piston alloys are mostly of near eutectic composition due to their excellent castability amongst other desirable properties imparted by Si [1]. These alloys are uniquely different from the more popular commercial Al-Si alloys (e.g., A356 and 319 type alloys) because of their high alloying content mainly designed to enhance formation of high temperature strengthening phases such the θ′-Al_2Cu, S′- Al_2CuMg, Al_3Ni and Al_3CuNi_2 [1,2]. The Ni content is these alloys is particularly high (0.5% to 2.5%) because of thermally stable strengthening phases that it forms [2]. It is particularly important to note that some patents suggest Fe levels of up to 2% to enhance formation of stable intermetallics for high temperature strength [3]. However, these high alloying content levels can impact negatively on the castability of these alloys. There is also a tendency to degrade room temperature mechanical properties as these intermetallics become potent crack initiation sites.

In most commercial Al-Si alloys, Fe is a common unwanted impurity that leads to formation of various types of Fe-rich intermetallic phases that deteriorate both their castability and mechanical performance. The most detrimental phase has often been identified as the β-Al_5FeSi because of its plate-like morphology. Addition of small amounts of elements such as Mn, Cr, Be, Co, and Sr is reported to lead to the formation of other phases with less harmful morphologies [4,5]. Mn is widely used at an Fe:Mn ratio of 2 although alternative levels have also been proposed [4,6]. Cr is less popularly used mainly due to concerns that it tends to form sludge although this is more likely to form only in diecastings because of low melt holding temperatures [4]. However, some researchers have shown that the use of Cr alone or in combination with Mn can be much more effective than using Mn alone [7,8]. Strontium and antimony are also often added to modify eutectic Si particles [9] but Sr has recently been shown to have a secondary effect of suppressing the formation of the β phase [10]. It is also reported to result in the fragmentation of the β-phase [11]. On the other hand, addition of Ti-based grain refiners have been reported to coarsen the β-phases [4,11].

These observations have however been reported mainly in the simpler commercial alloys and little information is available on their effect in piston alloys. It is not even clear whether such

elements would be necessary as the β-phases may not be a major problem in these alloys as it forms less frequently [12-14]. However, they may influence the formation of other phases such as Al_9FeNi, which are common in these alloys and reported to play a significant role in fatigue crack nucleation [14]. For reliable application of recycled piston alloys, it is necessary to have a clear understanding of the effect of these minor elements, which may be inadvertently present as impurities or deliberately added. The elements chosen for evaluation in this study are those commonly added to commercial Al-Si alloys for neutralization of Fe effects (Mn, Cr, and Sr), eutectic Si modification (Sr and Sb) and grain refinement (Al5TiB grain refiner). This paper discusses their effect on the mechanical properties of a secondary piston alloy.

2. Experimental Method

The alloy investigated was obtained by melting 70 kg of piston scrap in a graphite crucible furnace to 730˚C and thoroughly skimmed before pouring into 4 kg capacity ingot moulds. The chemical composition of the alloy was determined using inductively coupled plasma spectroscopy as 10.6%Si, 1.36%Cu, 1.08%Ni, 0.78%Mg, 1.06%Fe, 0.08%Mn, 0.03%Cr, 0.06%Ti, 0.02%Sn, 0.09%Zn, 0.04%K. The chemical composition of the alloy shows that it is equivalent to the AE413 alloy recently investigated by Daykin [9]. It is also equivalent to the British LM13 or Japanese AC8A piston alloys. The 4 kg ingot samples were charged into a graphite crucible and melted to 750^{o}C in an electric furnace under a cover flux and then skimmed. Further chemistry adjustments were done via addition of master alloys (e.g., Al-5Ti-1B or Al-10Sr) or compacted additives of Mn and Cr. Antimony was added as a pure metal in the form of granules. Eleven variants of this alloy were obtained by adjusting the level of the minor elements whose effect was under investigation. The alloy variants and their respective minor element levels were: P (no addition), P2Sr (0.02%Sr), P5Sr (0.05%Sr), PSb (0.2%Sb), PMn (0.53%Mn), PMnCr (0.3%Mn+0.2%Cr), P2SrGr (0.02%Sr+0.28%Al5Ti1B), P2SrMn (0.02%Sr+0.53%Mn), P5SrMn (0.05%Sr+0.53%Mn) and PCr (1.06%Cr). The melts were gently stirred to ensure complete dissolution and homogenisation. Degassing was achieved by bubbling nitrogen gas through the melt for 15 minutes using a ceramic tube. It was then skimmed and poured at 740^{o}C into a cast iron mould preheated to 470^{o}C. The base alloy (P) was poured without element addition after nitrogen degassing and skimming. A ceramic foam filter was used in the filling system to reduce liquid metal velocity and trap oxides or other inclusions remaining in the melt. The resulting bar castings were 200 mm long by 150 mm high and with a thickness varying from 10 mm at the bottom to 20 mm at the top designed to enhance feeding. The bars were sectioned into two parts with one part being subjected to a T6 heat treatment and the remaining piece analysed in its as-cast state. The T6 heat treatment schedule involved a solution treatment at 495˚C for 8 h followed by quenching in hot water at 80˚C and aging at 190˚C for 8 h without delay.

Samples for microstructure analysis were sectioned from a part of the casting that was about 15 mm thick. These were polished to OPS finish using conventional metallography and observed under an Olympus BH2 microscope and JEOL JSM 6500F SEM microscope fitted with an Oxford Inca 300 energy dispersive X-ray suite. An accelerating voltage of 15 kV was used. Furthermore, match stick samples of ~2x2x20 mm were scanned using an X-tek CT 160Xi micro-focus Computed Tomography (μCT) scanner. Optimal 1910 radiographs were taken through a 360 degree rotation at a filament current of 68 μA and an accelerating voltage of 68 kV using a molybdenum target. No filter was used and the CMOS detector used a frame rate of 2 fps and a digital gain of 1. The images were reconstructed to a 3D volume using the CTPro software. The volumes were analysed using VG Studio Max 2.0 and ImageJ to characterise the volume fraction (V_f) of intermetallics and porosity. The μCT data was also used to obtain the size and shape (α-aspect ratio) distribution of porosity using ImageJ. The resolution of the μCT images was ~5 μm and not adequate to analyse the size distribution of intermetallics. Instead, at least 10 backscattered (BEI) SEM images (at X150

magnification) were analysed for each alloy using ImageJ. The dendrite arm spacing (DAS) at the region of interest was measured using ImageJ and found to be approximately 28 μm. This corresponds to a cooling rate (R) of ~3.4°C/s as computed using the expression $\lambda=CR^{-\phi}$ (where, C=45.7, ϕ=0.4 and λ=28 μm) [7].

As-cast and T6 tensile test specimens were sectioned from the castings and prepared according to ASTM B108-82b with a gauge length of 25.4 mm and a diameter of 6.35 mm. The Samuel Denison Tensile testing machine was used to carry out the tests at a strain rate of 1 mm/min. Furthermore, impact testing was performed on unnotched 10x10x55 mm specimens in accordance with ASTM E-23 using a Torsee's Charpy Impact Testing Machine. The results are averages of three tests done for each alloy.

3. Results and Discussion

A detailed discussion of the influence of element addition on porosity and microstructure of this alloy is presented in a seperate paper in this conference [15]. However, some micrographs and quantitative data on porosity and intermetallics are reproduced here so as to provide context for a discussion on mechanical property results. For a start, the as-cast microstructure of the base alloy is shown in Fig. 1a in which the various phases observed are identified. A typical EDS spectrum of the β-Al_5FeSi phase is shown in Fig. 1b and the typical chemical compositions of the phases identified in Fig. 1a are also given. The Chinese script-like Mg_2Si phase was observed in the as-cast microstructures of all the alloys but dissolved during solution heat treatment. The Al_9FeNi phase also appeared abundantly in all alloys either as thick or thin plates and as interconnected acicular structures. The α-AlFeMnSi phases with a Chinese script morphology and β-Al_5FeSi platelets were observed to occur in the base alloy but less frequently. The Si particles appeared both as the primary blocky phase and as acicular eutectic particles. The edges of the Si particles tended to be rounded after heat treatment but the particles still maintained their unmodified structure.

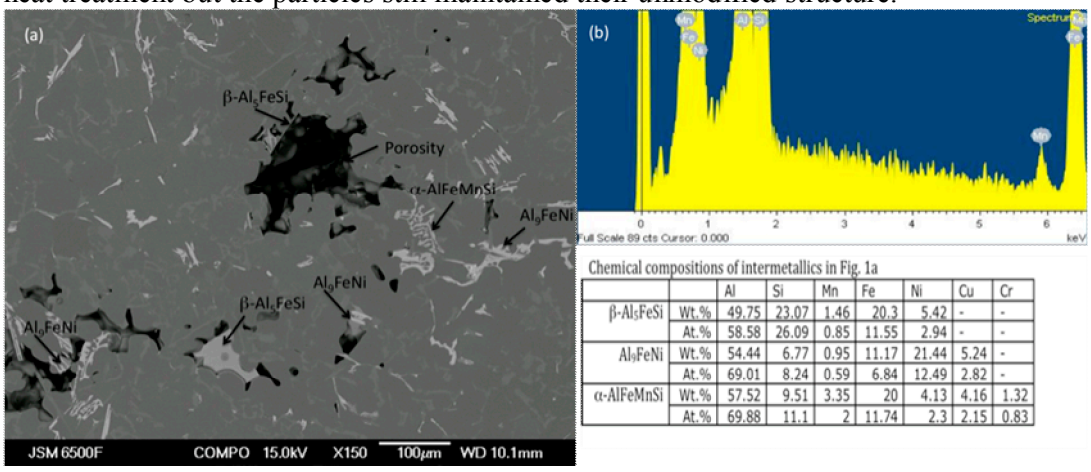

Chemical compositions of intermetallics in Fig. 1a

		Al	Si	Mn	Fe	Ni	Cu	Cr
β-Al_5FeSi	Wt.%	49.75	23.07	1.46	20.3	5.42	-	-
	At.%	58.58	26.09	0.85	11.55	2.94	-	-
Al_9FeNi	Wt.%	54.44	6.77	0.95	11.17	21.44	5.24	-
	At.%	69.01	8.24	0.59	6.84	12.49	2.82	-
α-AlFeMnSi	Wt.%	57.52	9.51	3.35	20	4.13	4.16	1.32
	At.%	69.88	11.1	2	11.74	2.3	2.15	0.83

Fig.1 Typical (a) SEM migrograph (BEI mode) of the base alloy showing β-Al_5FeSi, Al_9FeNi, α-AlFeMnSi and porosity interconnected with intermetallics, (b) EDX spectrum of the β phase and chemical composition of some of the phases observed.

In the 0.02%Sr and 0.05%Sr modified alloys, there were no primary Si particles and the eutectic Si appeared as a well modified fibrous structure (Fig. 2). However, in both alloys, the addition of Sr led to segregated regions of intermetallics in which the Si particles were partially modified. These regions were more apparent in the 0.05%Sr modified alloy as shown in Fig. 2a. The phases identified in these alloys included Mg_2Si (see Fig.2a), Al_9FeNi, λ-$Al_5Cu_2Mg_8Si_6$, $Al_3(CuNi)_2$ and the α-AlFeMnSi phase with dissolved Cr, Ni and Cu (Fig. 2b). Fewer β phases were observed in the 0.02%Sr alloy compared to the base alloy but none was observed in the 0.05%Sr alloy providing further confirmation of the suppression of this phase by Sr. Pores were also observed to be closely

linked with intermetallics in most alloys as shown in Figs. 1a and 2b. Note the 3D morphology of the Al_9FeNi, β-phase (see Fig 1a) and the λ-phase (Fig. 2b) exposed by porosity. This underscores the significance of all types of intermetallics in pore formation. The β-phase is reported to increase porosity via different mechanisms including physical blockage of feeding channels [4,5,16].

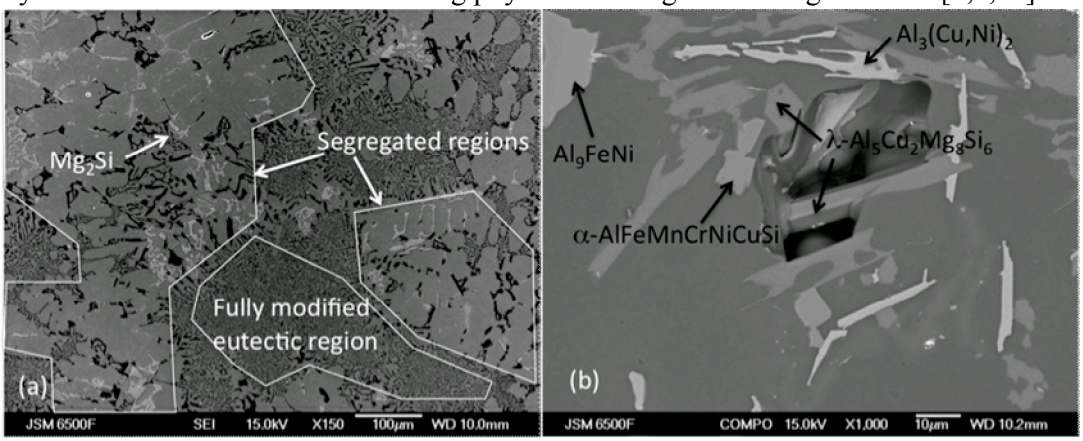

Fig. 2 (a) SEM micrograph of 0.05%Sr alloy in secondary mode (SEI) showing segregated regions of intermetallics and partially modified Si particles and other regions of fully modified Si. (b) SEM (BEI) of the alloy at high magnification showing identified intermetallic phases.

Table 1 shows a summary of the quantitative measurements of porosity and intermetallic characteristics in the alloys. The alloys are represented by their codes as given in section 2. The largest pores and intermetallics in each alloy were measured in terms of the maximum feret dimension (L_f) and the equivalent circle diameter (D_{eq}). The area fraction (A_f) of intermetallics was also measured from 2D images to compare with the 3D CT volume measurements. The V_f of intermetallics increased as expected with element addition except for 0.2%Sb alloy in which it reduced. This reduction may be associated with the preferential formation of thin β-phases in the alloy after Sb addition. The table shows that porosity was observed in all alloys but with different degrees of severity. It is clear that there is no apparent correlation between V_f, A_f, L_f, D_{eq}, and α. However, the table shows that the largest pores or intermetallics have low aspect ratios implying that they are irregularly shaped even in Sr-modified alloys in which several pores with rounded morphology were observed.

Table 2 Quantitative measurements of porosity and intermetallic characteristics in the various alloys

Pores	P	P2Sr	P5Sr	PSb	PMn	PCr	PMnCr	P2SrGr	P2SrMn	P5SrMn	PSbMn
V_f %	0.03	1.5	1.25	0.13	0.04	<0.01	0.04	1.21	0.38	1.33	0.48
Max. L_f	427	923	374	499	276	90	273	991	428	895	837
D_{eq}	185	390	143	197	89	37	131	528	224	416	104
α	0.103	0.056	0.083	0.057	0.181	0.238	0.334	0.132	0.273	0.056	0.166
Phases											
V_f %	10	13.2	12.6	9.3	13.7	14.9	13.5	12.8	14.2	15.7	13.3
A_f %	4.14	4.96	5.15	6.9	5.7	5.47	6.03	5.4	7.3	9.3	6.97
L_f	248	163	212	280	338	116	342	277	401	707	294
D_{eq}	76	52	76	82	84	52	91	104	71	94	99
α	0.008	0.12	0.028	0.032	0.006	0.122	0.008	0.008	0.008	0.022	0.011

Average trends in UTS, impact energy and % elongation values with various levels of element additions are shown in Fig. 3. The error bars indicate the scatter in the results. The base alloy recorded average as-cast UTS, impact energy and % elongation values of 140 MPa, 3.43 J and 2.3% while T6 values were 223 MPa, 4.15 J and 2.1%, respectively. Addition of up to 1% Cr caused the most significant improvement in the mechanical performance of the alloy. This addition caused an 18%, 96% and 61% increase in as-cast UTS, impact energy and % elongation respectively while in T6, the

increases were 16%, 75% and 43%. The high mechanical performance in the 1%Cr alloy is attributed to its low porosity (V_f<0.01) compared to all other alloys as shown in Table 1. Furthermore, the refinement of intermetallics with 1%Cr addition contributed significantly to this improvement. This alloy registered the lowest value of the largest intermetallic particle size (V_f=116 μm). Other significant improvents in mechanical performance were registered by addition of 0.53%Mn followed by the combined addition of 0.3%Mn+0.2Cr. These alloys had equivalent porosity and higher intermetallics levels compared to the base alloy. However, on average, the phases had compact morphologies compared to the base alloy and no β-Al_5FeSi particles were observed. The platelet morphology of the β-Al_5FeSi phase makes it particularly detrimental to mechanical properties [4,5] and may have played a significant role in the failure process of the base alloy.

All the other additions resulted in a significant increase in porosity and were expected to reduce mechanical properties especially ductility. However, slight improvements in ductility and impact energy were registered in all alloys both in as-cast and T6 conditions except for the 0.02S%Sr+0.28%Al-5Ti-1B alloy in which their was a drop in impact energy. This observation is counter-intuitive and can only be interpreted by the statistical nature of mechanical properties porosity data. Previous work [17] has also shown that their is no direct correlation of tensile properties with volume fraction porosity. Instead it was shown that tensile properties correlate well with the area fraction of porosity on the fracture surface. This was related to the reduction in the load bearing area of the specimens. However, definite trends of tensile properties with average area fraction porosity have recently been reported [18]. However, no such trend was observed in our work. It is however significant to note that the as-cast tensile strength reduced in the 0.02%Sr+0.28%Al-5Ti-1B, 0.02%Sr+0.53%Mn, 0.05%Sr+0.53%Mn and 0.2%Sb+0.53%Mn alloys. All these alloys had higher porosity than the base alloy as shown in Table 1. This emphasizes the statistical nature of the relationship between mechanical properties and average porosity. More data and use of statistics of extrema may be required establish trend between overall pore characteristics and tensile properties. The improvement in tensile strength after T6 treatment further indicates that porosity was not the overriding factor in mechanical performance even in cases where it is higher. Heat treatment to the T6 condition strengthens the matrix and tends to dissolve or spheroidise certain phases. This generally leads to increased mechanical performance especially when porosity is low. This has long been recognised [19].

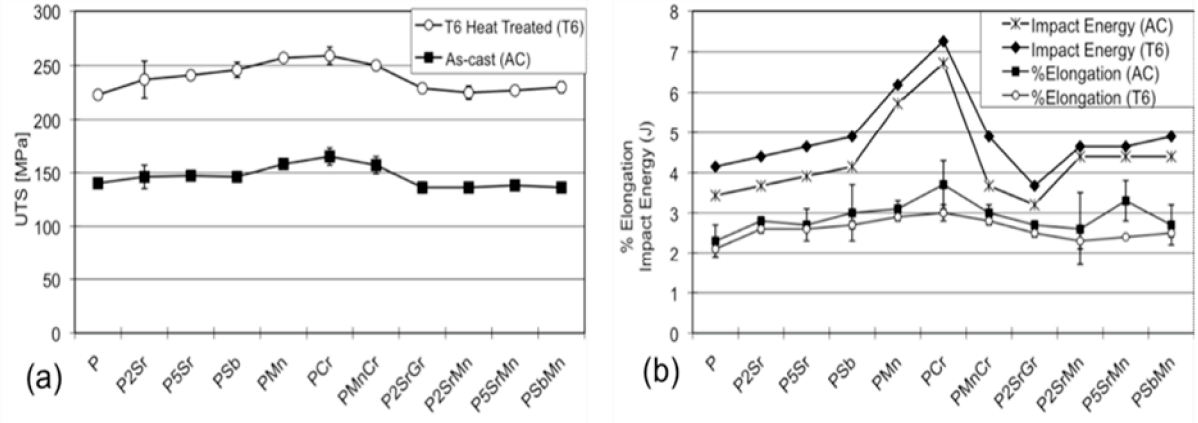

Fig. 3. Variation of average as-cast (AC) and heat treated (T6) (a) ultimate tensile strength (UTS), and (b) impact energy and % elongation of the alloy with minor element additions.

The study revealed that among the elements added to the base alloy, Cr caused the most significant improvement. This occurs even at the high Fe:Cr ratio of 1, which is much higher than those previously recommended such as Fe:Cr of 3 suggested by Mahta et al. [20]. Gustafsson et al. [7] reported that while addition of either Mn or Cr will be beneficial to Al-Si alloys in changing the harmful intermetallic phases to less harmful phases, Cr addition could be more beneficial than Mn. Based on their work and current results, it is apparent that more attention needs to be paid to the use of

Cr as an alternative to Mn even in piston alloys. Sludge formation may not be an issue in processes other than diecasting [4].

4. Conclusion

The effect of minor element additions (Sr, Sb, Mn, Cr and Al-5Ti-1B grain refiner) on the mechanical performance of a secondary cast aluminium piston alloy, with 1 wt.% Fe was investigated. It was observed that addition of even high levels of Cr of up to 1% was better than a 0.53%Mn addition in improving the tensile strength, impact energy and % elongation of the alloy. The high mechanical performance recorded in the 1%Cr alloy was attributed to its low porosity compared to all other alloys and the fine compact intermetallics observed in the alloy. Other additions also resulted in improved mechanical properties with 0.53%Mn performing better than 0.3%Mn+0.2%Cr while the rest recorded marginal improvements.

Acknowledgements

The authors acknowledge the assistance of Allan Barber of LSM and Carole of Blackwell & Graham as well as ALEASTUR of Spain. Jomo Kenyatta University of Agriculture and Technology and the University of Nairobi are also acknowdged for their contributions to this work.

References

[1] J.A. Lee and P-S. Chen: US Patent, No.US 6918970 B2, July, 2005
[2] J. Barnes and K. Lades. SAE Trans., Paper No. 2002-01-0493
[3] A. Tahinata, N. Sato, H. Kutsumata and T. Shiraishi: US Patent, No. US 7398754 B2, July, 2008.
[4] P.N. Crepeau: AFS Trans. 103 (1995) 361-366.
[5] T. O. Mbuya, B. O Odera and S. P. Ng'ang'a: Int. J. Cast Met. Res. 16 (5) (2003) 451–465.
[6] J.Y. Hwang, H.W. Doty and M. J. Kaufman: Mater. Sci. Eng. A, 488 (2008) 496-504.
[7] G. Gustafsson, T. Thorvaldsson and G. L Dunlop: Metall. Trans. A. 17A (1986) 45-52.
[8] H.Y. Kim, W. H. Sang and H. M Lee: Mater. Lett. 60 (2006) 1880-1883.
[9] M. Garat, G. Laslaz, S. Jacob, P. Meyer and R. Adam: AFS Trans., 100 (1992) 821-832.
[10] S.G. Shabestari, M. Mahmud, M. Emamy & J. Campbell: Int. J. Cast Met. Res. 15 (2002) 17-24.
[11] A.M. Samuel, F.H. Samuel and H.W. Doty: J. Mater. Sci. 31 (1996) 5529-5539.
[12] C.R.S. Daykin: *Microstructural Modelling of Commercial Aluminium-Silicon Alloys for Piston Applications*, PhD Thesis, University of Cambridge, 1998.
[13] Z. Qian, X. Liu, D. Zhao and G. Zhang, Mater. Lett., 62 (2008) 2146-2149.
[14] C.L. Chen, *Characterisation of Intermetalic Phases in Multicomponent Al-Si Alloys for Piston Applications*, PhD Thesis, IPTME, Loughborough University, 2006.
[15] T.O. Mbuya. I. Sinclair, B.R. Mose, S.M. Maranga and P.A.S. Reed: Appearing in this conference.
[16] M.A. Moustafa: J. Mater. process. Technol., 209 (2009) 605-610).
[17] C.H. Caceres and B.I. Selling: Mater. Sci. Eng., A220 (1996) 109-116.
[18] Z. Ma, A.M. Samuel, F.H. Samuel, H. Doty and S. Valtierra: Mater. Sci. Eng. A490 (2008) 36-51.
[19] J.A. Eady and D. M. Smith: Mater. Forum 9 (1986) 217
[20] M. Mahta, M. Emamy, A. Daman A Keyvani and J Campbell: Int. J. Cast Met. Res., 18(2) (2005) 73-79.